that the star is not pathological in any way. We then demonstrate that its X-ray flux is, indeed, variable. However, because the current observations do not span half of a rotation period, we cannot determine whether the variability is is cyclic or secular in nature.

Subject headings: stars: early-type – stars: winds – x-ray: stars

really want to start with this
general x-ray/O star background?
(could in any case, tighten it up)

1. Introduction

With the launch of *Chandra* and *XMM*, true X-ray spectroscopy became possible. With these new data, it quickly became apparent that the observed X-ray line profiles of O stars (e.g., Waldron & Cassinelli 2001, Cassinelli et al. 2001, Rauw et al. 2002, Miller et al. 2002) did not conform to expectations for a spherically symmetric homogeneous wind with the accepted O star mass loss rates (Ignace & Gayley 2002, Owocki & Cohen 2001). Even more sophisticated profile fitting techniques could not resolve the disagreement (Kramer et al. 2003, Leutenegger et al. 2006, Cohen et al. 2006). This quandary lead to the development of different models, most notably those with winds that are highly fragmented (Feldmeier et al., 2003, Oskinova et al., 2004 and Owocki & Cohen, 2006). While these models can, in fact, fit the the observed profiles with the expected mass loss rates, some reservations about their physical basis or broader implications have been raised (Owocki & Cohen 2006).

A different, perhaps related, aspect of O star winds is that all O stars which have been observed over time scales of a day or more demonstrate UV wind line variability (e.g., Kaper et al. 1996, 1999). This phenomenon suggests the presence of structures in their winds and that some of these structures must be quite large. To see this, consider a star of radius $R_\star$ whose UV wind lines varies by 10% (most observed variations are larger than this). It is easy to show that the structure responsible for the variability must be $\gtrsim 0.3R_\star$. These results lead Cranmer & Owocki (1996) to model wind variability by large spiral structures known as Co-rotating Interaction Regions (CIRs, Mullan, 1986). Building upon this idea, Mullan & Waldron (2006) introduced a qualitative model for the X-ray emission which is largely based on the presence of CIRs in the winds.

One major problem with CIR based models is that periodic variability of the X-ray fluxes of normal, single O stars is expected, but none is observed. However, one must keep in mind that there are considerable obstacles to observing such variability and establishing a link between it and UV wind lines variability for single, normal O stars. First, the CIRs are thought to be confined to the equatorial plane. Consequently, variability may not be seen unless our line of sight to the star happens to be nearly equator-on. Second, wind variability appears to be related to the stellar

[1]Based on observations made by the *Chandra* X-ray Observatory Center, which is operated by the SAO on behalf of NASA under contract NAS8-03060.

rotation period (Prinja 1988). Since the rotation periods of most O stars are several days, these are much longer than the typical X-ray observation and the variability may not be detected. Third, there are only a few stars which have been observed in the UV over long enough intervals for good wind line periods to be identified, and such a period is needed to claim a definite connection between X-ray and UV wind line variability . Fourth, there are very few normal stars whose X-ray fluxes are strong enough to be observed with current instrumentation.

The O7 III(n)((f)) star ξ Per is an ideal candidate for attempting to make a connection between UV wind line and X-ray variability. First of all, ξ Per appears to be a perfectly normal O7 giant (see, Walborn 1973, and Walborn et al. 1985, for descriptions of its optical and UV spectra, respectively). Its only destinguisning feature is that is that it has a somewhat high (but not abnormal) rotational velocity $v \sin i = 204$ km s^{-1} (Penny, 1996). Because of its moderate $v \sin i$, its expected rotation period is short enough to be captured by a time series of manageable duration. This was done in a detailed study of its UV and optical line variability by de Jong et al. (2001). They demonstrated the presence of a well characterized, distinctive 2.08 d period in the UV wind line variability. This turns out to be roughly half of the expected rotation period if the star is viewed nearly equator-on (see their Figure 4). Further, they were able to model the variability by two sets of two armed CIRs (see, their Figure 17), with one set of arms dominating the variability. These properties of ξ Per, together with its relative brightness at X-ray wavelengths, make it an ideal candidate to determine whether the CIRs that are thought to modulate the UV wind lines in this star (and possibly all luminous OB stars with massive winds) might modulate the its X-ray flux as well. To pursue this conjecture, we obtained a 162 ks (0.45 rotation periods and 0.90 periods of the strong CIR activity) *Chandra* observation of ξ Per.

In §2, we describe the observations. In §3, analyze the mean X-ray profiles and the time dependence of the X-ray flux of the star. In §4, we discuss and summarize our results.

2. The Observations

Although a continuous observation of 2.1 d is required to be certain that the full range of variability is observed, as one arm of the CIR pattern traverses our line of sight, the maximum visibility of ξ Per to *Chandra* was $\sim$ 162 ks (1.9 d), or roughly 90% of the UV wind line modulation period. The observations were obtained with *Chandra*'s transmission High Energy Transmission Grating Spectrometer (HETGS) and began on 2004 March 22.

The HETG consists of two sets of gratings; the Medium Energy Grating (MEG) and the High Energy Grating (HEG). The events were recorded on the ACIS-S chips and consist of a ± 1 order dispersed spectrum for both the MEG and HEG and a directly transmitted, zeroth order, image. Some spectral information can be extracted from the zeroth order image through the energy determined for the individual events (see, the *Chandra* Observatory Guide xxxx for further details). All of the data were processed with version 3.2 of the *Chandra* Interactive Analysis of Observations

we don't need this

could start our Xray text here (since it starts w/ a description of the reduction)

(CIAO) software package.

The HEG spectrum is barely detectable for our target, and will not be considered further. On the other hand, the MEG spectrum is well suited to spectral line analysis. In contrast, zeroth order image contains little spectral information, but is better suited for time series analysis. This is because the X-ray background is uniformly distributed over the detector and the zeroth order image cover a much smaller detector area than the first order spectra but contains comparable counts. If we simply select events with *ASCA* grades of 6 or less and energies ≥ 3 kev, then we find 6246 and 10709 events for the zeroth and ± 1 order spectra, respectively. Since the ± 1 order spectra cover many times larger are than the zeroth order spectrum, it is clear that the latter is much better suited for time series analysis.

Pile-up (the arrival of two photons near the same location between CCD reads) was not a major issue for the observations. As we shall see, the strongest lines in the MEG spectra only had count rates of $\lesssim 1.0 \times 10^{-3}$ cps and the count rate of the zeroth order image was $\lesssim 0.04$ cps. In the first case, pile-up is completely negligible, and in the latter it never exceeds 5%.

3. Analysis

The analysis consists of two parts. In the first part, we analyze the mean X-ray profiles and in the second part we search for variability in the total X-ray flux from the star.

3.1. Analysis of the Profiles

The combined ± 1 first order MEG spectrum is plotted in units of counts per 0.005Å bin in Figure 1. Overall, the spectrum is typical of mid-O stars (e.g., see Cohen et al. 2006). To obtain a quantitative measure of the X-ray properties of ξ Per, we use the model developed by Owocki & Cohen (2001) to fit the strongest Ly α transitions: O VIIIλ18.97, and Fe XVIIλ15.01. These models provide estimates for the minimum radius of the onset of the emission, the power in a power law distribution of the emitting gas density and the opacity of the overlaying wind material. The fits were performed in the same manner described by (Kramer et al. 2003) and are shown in Figure 2 and the results are listed in Table 1 (see, Kramer et al. for details of the analysis).

In addition to the isolated Ly α lines, Leutenegger et al. (2006) have extended the Kramer et al. (2003) analysis to include the He-like *fir* complexes. In this case, additional information about the location of the X-ray emitting plasma can be determined from the f/i ratios, since it is sensitive to the intensity of the photopheric radiation field, and this field is diluted at larger distances from the star. Figure 3 shows the fit to the Mg XI λ9.2 *fir* complex (the only set of *fir* lines in the current ξ Per spectrum with adequate signal to allow detail modeling), and Table 1 lists the results. The details of the modeling follow those described by Leutenegger et al.

The results of this analysis are the following: First, the fits to individual strong Ly α-like lines are consistant with a generic wind-shock scenario, but with effective optical depth reductions of an order of magnitude relative to that expected from expectations – conclusions are similar to those reached for ζ Pup (Kramer et al. 2003) and ζ Ori (Cohen et al. 2006), second, the modeling of the He-like *fir* lines demonstrates that the formation radius is consistent with wind-profile fits – an onset of X-ray emitting plasma occurring at 1.5 to 2 R_* (similar to Luetenegger et a. 2006).

In summary, the results listed in Table 1 are typical of normal O stars, and imply a clumped or structured wind (see, Owocki & Cohen 2006).

3.2. Analysis of the Variability

We begin the time series analysis by "rotating", i.e. relabeling, the x and y sky coordinates by $\theta = -29.31°$, to produce a prime coordinate system given by $x' = x\cos\theta + y\sin\theta$ and $y' = -x\sin\theta + y\cos\theta$. In the prime system, the first order MEG spectra are aligned with the y'-axis, simplifying the analysis. Next, we impose an additional constraint for events to be accepted as part of the first or zeroth order images. We require them to lie within the strip defined by $2021 \leq x' \leq 2034$, and the zeroth order events are further constrained to lie within $5484 \leq y' \leq 5492$, and the ± 1 order events are excluded from this region. With these additional constraints (along with those imposed previously, i.e., *ASCA* grade ≤ 6, energies ≤ 3 kev), we find 5934 and 5981 events for the zeroth and ± 1 order spectra, respectively. These constraints apply to all of the counts analyzed in this section.

do you really want to provide this much detail?

As an initial test for X-ray flux variability, we applied the Kolmogorov-Smirnov test to counts which fell into the region we define as the zeroth order image and first order spectra. This test gave probabilities of 1.00000 and 0.99977, respectively, that the data were time variable. The difference between the two results probably arises because the first order spectra contain considerably more background contamination. Consequently, we concentrated our temporal analysis on the zeroth order series.

To begin, we binned the data into 30 min. bins. For the zeroth order image, these bins all contain 50 or more counts, making it reasonable to approximate the intrinsic Poisson statitics of the X-ray photons by Gaussian statistics. We then determined the time dependence of the background affecting the zeroth order. This was done by first calculating the background for the region surrounding the zeroth order. Specifically, we included all counts within 200×200 pixel region centered on the zeroth order image, excluding the 20×20 pixel region centered on it. Next, we examined all of the counts on the CCD containing the zeroth order image, excluding a 20 pixel wide strip which contains the zeroth and fist order images. Both results were normalized by their areas and then multiplied by the area of the zeroth order image to obtain estimates of the background rates affecting the zeroth order image. The results are shown in Figure 5. We see that the two background rates agree, so we can be confident in using the more well-determined

background from the larger region.

We then subtracted the background rates from the zeroth order rates (the background actually has a very small effect on the result) and used ordinary least squares to determine a linear fit to the data, counts $s^{-1} = a_1 t + a_2$. The fit to the zeroth order counts minus the background is shown in Figure 2 and the fit parameters are listed in Table 6. The Table lists the best fit parameters and their formal errors, the reduced χ^2 per degree of freedom, N_D, and the probability that this statistic is greater than or equal to the observed value. The results show that the slope (i.e., the linear trend in the data) is extremely well-defined (at the 5σ level) and that the X-ray flux changed by more than 25% over the course of the observation.

We also fit two simple, heuristic models to the time series resampled into 2 hour bins. These were: a trigonometric model, to search for evidence of repeatability, and; an exponential decay model, to characterize the recovery from an episodic event. Specifically, these models are given by

$$\text{counts s}^{-1} = a_1 \cos(\frac{t}{2\pi P} + a_2) + a_3 \ , \text{ and} \quad (1)$$

$$\text{counts s}^{-1} = a_1 e^{-t/a_2} + a_3 \quad (2)$$

where P is fixed at 2.08d (deJong et al. 2001). The results of this exercise are shown in Figure 7 and are summarized in Table 2. The sinusoidal fit is not formally better than the linear fit. The exponential fit is a better data than the other two, even though its parameters are poorly defined. In contrast, the sinusoidal fit is the poorest, and its parameters are quite well defined. However, none of the models is strongly favored over the others, so there is no compelling reason to adopt any one of them to characterize the variability.

Finally, we examined the time dependence of the hardness ratio. We chose to divide the spectrum into two bands: a "soft" band for events with energies in the range, $0.4 \leq e < 0.8$kev, and; a "hard" band for events with energies in the range $0.8 \leq e < 3.0$kev. This division gave roughly equal numbers of events to both bands. We then examined the time dependence of the data (in 2 hour bins) for variability. The errors affecting the ratios were calculated by standard propagation of errors techniques, since there are adequate counts within each bin to approximate Poission statisitics by Gaussian distributions. The ratio of the soft to hard bands are shown in Figure 8. The weighted mean and standard deveation of this series are 1.147 and 0.143, respectively. These were used to calculate a reduced χ^2 statistic $\sqrt{\chi^2/N_D} = 1.146$ where $N_D = 23$. The probability of the ratio being constant is then 15%. So the ratio may be variable, but no distinct trend can be determined from these data.

4. Discussion

Our results from §3 demonstrate that the X-ray line profiles of ξ Per are typical of other O stars which have been analyzed. This result is reinforced by Walborn's (2006) assessment of the X-ray spectrum of ξ Per, where he finds that its spectral morphology fits seamlessly into the sequence

In general, I think the Disussion needs some work

of normal O star X-ray spectra. However, unlike other, normal O stars, the integrated X-ray flux from ξ Per decreased by $27 \pm 7\%$ over a period of 44.4 hours. Unfortunately, because were unable to observe it for one entire period. Figure 9 shows the observed variability repeated on the 2.08 d UV wind period. While this appears to be a plausible light curve (compare it to the H α light curve given by Morel et al. 2004 in their Fig. 3) a periodic fit to the data is no better than a linearly decreasing one. On the other hand, if the variability is part of some sort of episodic event (which provides the best fit to the data, although not by a significant factor), this event must have a considerably larger amplitude than the change we observe. This is because the X-ray flux does not appear to be asymptoting to an equilibrium level, and we certainly did not observe the onset of an event. Consequently, at this time we cannot determine whether the variation is due to secular changes or to rotational modulation.

```
*********************************************
This next bit will change depending on the optical data
*********************************************
```

We had planned contemporaneous H α observations to determine the phase of the rotational modulation at the time of the X-ray observations, but we were unable to obtain inadequate time coverage due to poor weather conditions.

X-ray variability has been detected in a number of O stars (see, Skinner et al. 2005 for a recent summary). Activity with a time scale days has typically been related to magnetic or orbital processes. In a few cases, short period (hours) variability has been attributed random processes in a clumped wind. Of importance here, are two non-magnetic O stars which are variable on time scales that might be related to their stellar rotation peiods. These are the rapidly rotating O9.5 Vnn star ζ Oph (Oskinova et al. 2001) and the O star O5 III: n(f) star HD 150136 (Skinner et al. 2005). ζ Oph was observed for ~ 1.2 days and its X-ray flux was found to vary by about 20%. Further, this variation appears to repeat with a period of about 0.77 days, similar to its rotation period and to a period previously determined from its UV wind lines (0.875 ± 0.167 days) by Howarth et al. (1993). The X-ray flux from HD 150136 was observed to vary by 38% over a span of nearly 3 days. HD 150136 has not been well observed in the UV and its X-ray light curve was not observed to repeat. Nevertheless, as with ξ Per, the X-ray variability is large, and has a time scale that is consistent with the expected rotation period of the star.

Thus, we are left with two possible explanations for the observations. Either the X-ray flux of ξ Per experiences epsiodic flux changes which can be quite large (even though it appears to be a normal star), or else its X-ray flux is strongly modulated by rotating structures. If the latter is correct, then we would suspect that the only reason it we do not observe similar variability is other O stars is that we do not view them at an opportune angle, or have not observed them over a large enough portion of their rotation period. It is important to establish which of these alternatives is correct. In particular, if the flux is modulated, that could have wide ranging implications for the structure of O star winds.

Oskinova, L.M., Clarke, D. & Pollock, A.M.T. 2001, A&A, 328, L21

Owocki, S.P. & Cohen, D.H. 2001, ApJ, 559, 1108

Owocki, S.P. & Cohen, D. H. 2006, ApJ, 648, 565

Penny, L.R. 1996, ApJ, 463, 737.

Prinja, R. K. 1988, MNRAS, 231, 21P

Rauw, G., Blomme, R., Waldron, W.L., Corcoran, M.F., Pittard, J.M., Pollock, A.M.T., Runacres, M.C., Sana, H., Stevens, I.R. & Van Loo, S. 2002, A&A, 394, 993

Skinner, S.L., Zhekov, S.A., Palla, F. & Barbosa, C.L.D.R. 2005, MNRAS, 361, 191

Walborn, N.R. 1973, AJ, 78, 1067

Walborn, N.R. 2006, in the "proceedings of the Joint Discussion 4 at the IAU General Assembly, Prague, August 16-17, 2006". Editorial of the Universidad Complutense de Madrid, eds. Ana Ines Gomez de Castro and Martin Barstow

Walborn, N.R., Nichols-Bolin, J. & Panek, R.J. 1985, *International Ultraviolet Explorer Atlas of O-type Spectra from 1200 to 1900 Å*, (NASA Ref. Pub., 1155)

Waldron, W. L. & Cassinelli, J. P. 2001, ApJ, 548, L45

This preprint was prepared with the AAS LaTeX macros v5.2.

Table 1: Wind profile model parameters fit to the data.

Ion	λ_o (Å)	q	R_{min}/R_*	τ_*	Goodness of fit[a]
O VII	21.804, 21.602	$-0.30^{+.27}_{-.19}$	$1.66^{+.15}_{-.13}$	$0.06^{+.14}_{-.06}$	0.33
O VIII	18.969	$-0.12^{+.29}_{-.22}$	$1.61^{+.14}_{-.12}$	$0.26^{+.20}_{-.13}$	0.67
O VII	18.627	$0.39^{+1.38}_{-.71}$	$1.29^{+.29}_{-.18}$	$1.34^{+1.86}_{-.74}$	0.49
Fe XVII	17.051, 17.096	$-0.41^{+.29}_{-.19}$	$1.28^{+.21}_{-.13}$	$0.76^{+.52}_{-.33}$	0.40
O VIII	16.006	$-0.41^{+.41}_{-.31}$	$1.51^{+.98}_{-.25}$	$0.27^{+.48}_{-.19}$	0.53
Fe XVII	15.014	$-0.47^{+.22}_{-.16}$	$1.37^{+.15}_{-.14}$	$0.58^{+.41}_{-.25}$	0.29
Ne X	12.134	$-0.50^{+.35}_{-.21}$	$1.55^{+.32}_{-.21}$	$0.45^{+.46}_{-.29}$	0.14

[a]Fraction of Monte Carlo simulated datasets that gave a C statistic as good or better than that given by the best-fit model and the data. This can be interpreted as a rejection probability. Lower values indicate better fits.

replace

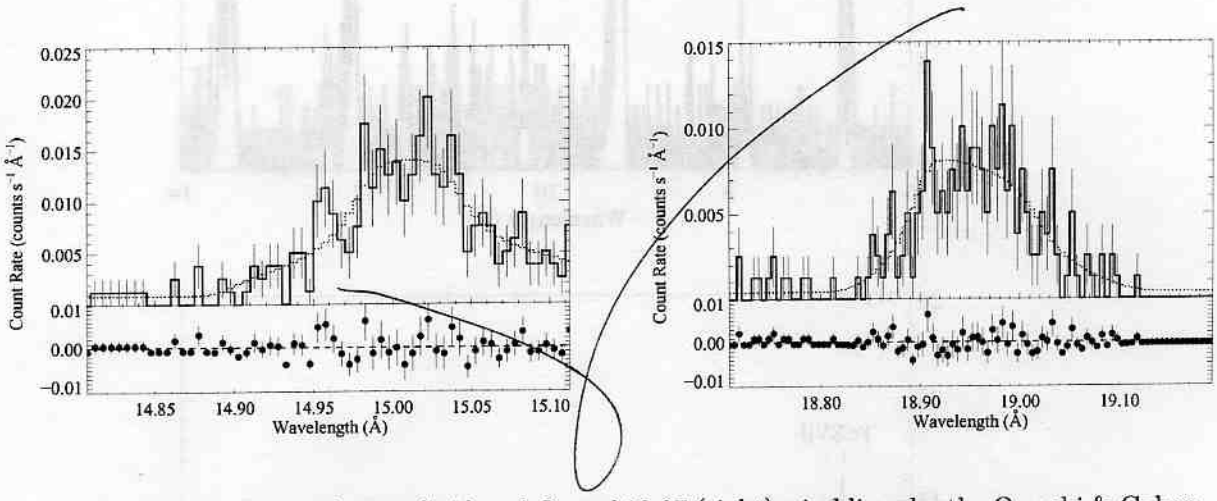

Fig. 2.— Fits of the Fe XVIIλ15.01 (left) and O VIIIλ18.97 (right) wind lines by the Owocki & Cohen (2001) model. The upper panel shows the fits, where the data are represented as histograms, the $\pm 1\sigma$ errors by vertical lines and the fits are the dashed curves. The lower panels shows the residuals and the $\pm 1\sigma$ error bars. The fit parameters are listed in Table 1.

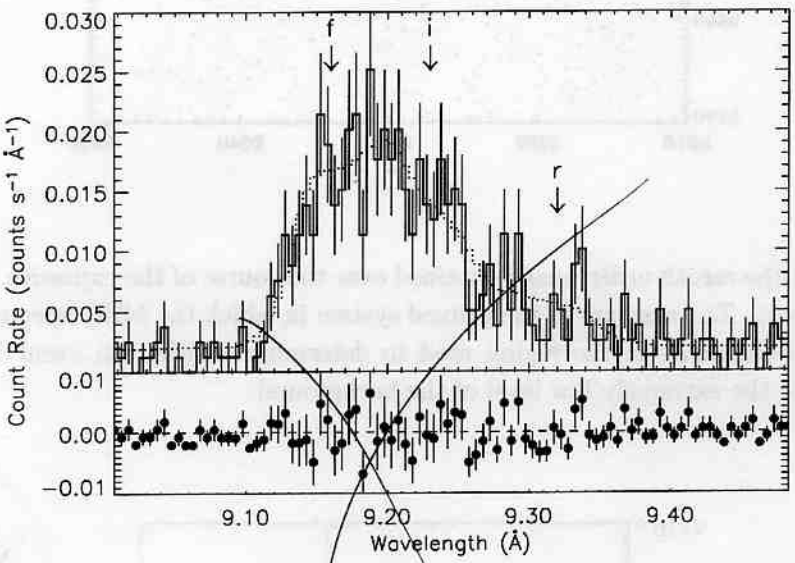

Fig. 3.— Fit of the Owocki & Cohen (2001) model to the Mg XI λ9.2 *fir* wind lines. The upper panel shows the fit, with the data represented as a histogram, the $1 \pm 1\sigma$ error bars by vertical lines and the fit by the dashed curve. The lower panel shows the residuals and $1 \pm \sigma$ error bars. The rest positions of the forbidden, intercombination and resonance components are indicated in the Figure by f, i, and r, respectively. The fit parameters are listed in Table 1.

replace

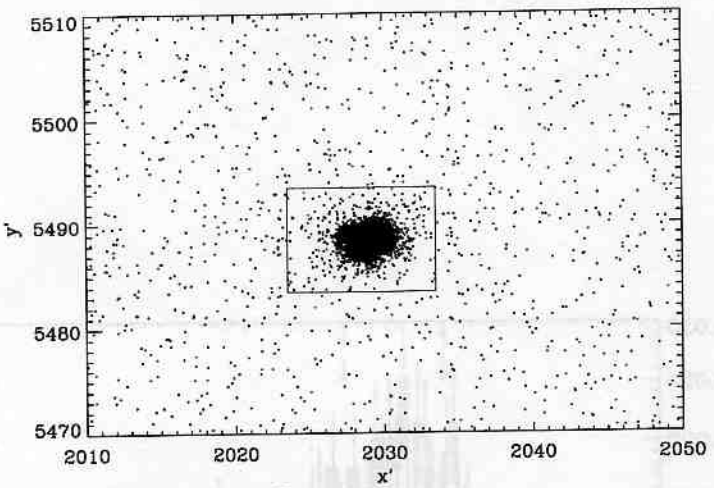

Fig. 4.— Counts in the zeroth order image obtained over the course of the exposure. Each count is represented by a point. The axes are in the primed system in which the MEG spectrum is vertical. We also show the boundaries of the region used to determine whether an event belongs to the zeroth order. Notice the extremely low level of the background.

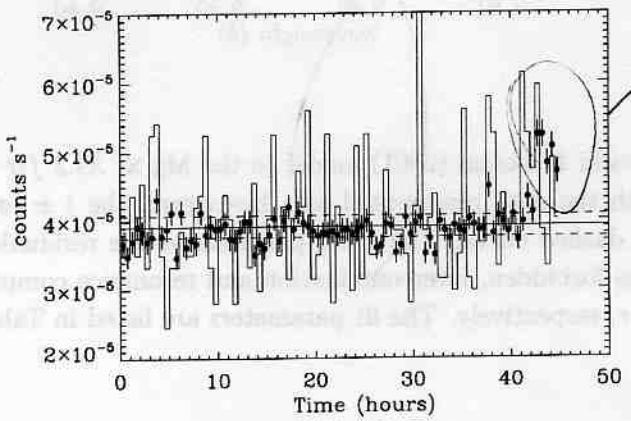

a little weird rise at the end

Fig. 5.— Count rates for backgrounds (in 30 min. bins) over the entire CCD that contains the zeroth order image (points) and for a region near the image (histogram) (both scaled to the number of pixels in the zeroth order image). This shows that the background is stable over the entire CCD.

#1 think it's a non-standard choice to show these 2 figures, the next one should be sufficient